biomolecules

MDPI

Article

Homogeneous, Synthetic, Non-Saccharide Glycosaminoglycan Mimetics as Potent Inhibitors of Human Cathepsin G

Daniel K. Afosah [1,2,*], Rawan M. Fayyad [1,2], Valerie R. Puliafico [3], Spencer Merrell [3], Eltice K. Langmia [3], Sophie R. Diagne [4], Rami A. Al-Horani [5] and Umesh R. Desai [1,2]

[1] Department of Medicinal Chemistry, School of Pharmacy, Virginia Commonwealth University, Richmond, VA 23298, USA; fayyadr@vcu.edu (R.M.F.)
[2] Institute for Structural Biology, Drug Discovery and Development, Virginia Commonwealth University, Richmond, VA 23219, USA
[3] Department of Chemistry and Biochemistry, Washington and Lee University, Lexington, VA 24450, USA
[4] Department of Chemistry, Virginia Commonwealth University, Richmond, VA 23298, USA
[5] Division of Basic Pharmaceutical Sciences, College of Pharmacy, Xavier University of Louisiana, New Orleans, LA 70125, USA
* Correspondence: afosahd@vcu.edu; Tel.: +1-(804)-828-7575

Abstract: Cathepsin G (CatG) is a pro-inflammatory neutrophil serine protease that is important for host defense, and has been implicated in several inflammatory disorders. Hence, inhibition of CatG holds much therapeutic potential; however, only a few inhibitors have been identified to date, and none have reached clinical trials. Of these, heparin is a well-known inhibitor of CatG, but its heterogeneity and bleeding risk reduce its clinical potential. We reasoned that synthetic small mimetics of heparin, labeled as non-saccharide glycosaminoglycan mimetics (NSGMs), would exhibit potent CatG inhibition while being devoid of bleeding risks associated with heparin. Hence, we screened a focused library of 30 NSGMs for CatG inhibition using a chromogenic substrate hydrolysis assay and identified nano- to micro-molar inhibitors with varying levels of efficacy. Of these, a structurally-defined, octasulfated di-quercetin NSGM **25** inhibited CatG with a potency of ~50 nM. NSGM **25** binds to CatG in an allosteric site through an approximately equal contribution of ionic and nonionic forces. Octasulfated **25** exhibits no impact on human plasma clotting, suggesting minimal bleeding risk. Considering that octasulfated **25** also potently inhibits two other pro-inflammatory proteases, human neutrophil elastase and human plasmin, the current results imply the possibility of a multi-pronged anti-inflammatory approach in which these proteases are likely to simultaneously likely combat important conditions, e.g., rheumatoid arthritis, emphysema, or cystic fibrosis, with minimal bleeding risk.

Keywords: allosterism; cathepsin G; glycosaminoglycans; mimetics; inflammation

check for updates

Citation: Afosah, D.K.; Fayyad, R.M.; Puliafico, V.R.; Merrell, S.; Langmia, E.K.; Diagne, S.R.; Al-Horani, R.A.; Desai, U.R. Homogeneous, Synthetic, Non-Saccharide Glycosaminoglycan Mimetics as Potent Inhibitors of Human Cathepsin G. *Biomolecules* **2023**, *13*, 760. https://doi.org/10.3390/biom13050760

Academic Editor: George Kokotos

Received: 12 April 2023
Revised: 25 April 2023
Accepted: 25 April 2023
Published: 27 April 2023

Copyright: © 2023 by the authors. Licensee MDPI, Basel, Switzerland. This article is an open access article distributed under the terms and conditions of the Creative Commons Attribution (CC BY) license (https://creativecommons.org/licenses/by/4.0/).

1. Introduction

Human cathepsin G (CatG) is a member of the neutrophil serine proteases (NSPs), a group of proteins released from the azurophilic granules of neutrophils. These proteases, which also include human neutrophil elastase (HNE), proteinase 3 (PR3), and neutrophil serine protease 4 (NSP4), are most associated with the host defense mechanism against pathogens [1]. Mature CatG is made up of 235 residues [2], and similar to the other NSPs, has an overall positive charge due to an abundance of basic residues (Figure 1) [3]. CatG has broad substrate specificity which affords additional roles, including the degradation of extracellular matrix; activation of matrix metalloproteases; processing and release of cytokines, chemokines, and growth factors; activation of caspases; generation of angiotensin II; and activation of platelet receptors [4–12]. Owing to this, nature has devised several physiological inhibitors, including α_1-antichymotrypsin, α_1-proteinase inhibitor, α_2-macroglobulin, serpin B1, proteinase inhibitor, and secretory leukocyte protease inhibitor, that regulate its

activity [13]. Recently, the role of NSPs in the inflammatory process has garnered a lot of attention because it is becoming clear that runaway inflammation arises from dysregulation of the natural protease–antiprotease balance [14–17].

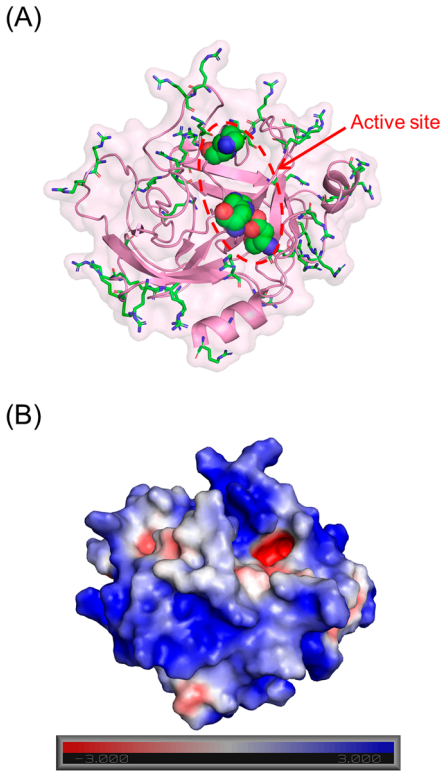

Figure 1. Structure of human CatG (PDB ID = 1 KYN). (**A**) shows that basic (sticks) and catalytic triad residues (spheres) of CatG include His57, Asp102, and Ser195 residues (chymotrypsin numbering). (**B**) shows the nature of electrostatic surface of the protease. Red and blue represent electronegative and electropositive surfaces, respectively.

CatG plays important roles in multiple inflammatory diseases including, rheumatoid arthritis [18], psoriasis [19,20], chronic obstructive pulmonary disease (COPD) [21,22], emphysema [23], and cystic fibrosis (CF) [24]. Elevated CatG expression is one of the causative disruptors of the natural protease–antiprotease balance, and is typically observed in these conditions. More importantly, high enzyme activity sets in motion the degradation of the connective tissue and ECM proteins, while also promoting apoptosis and activation of other pro-inflammatory mediators [13]. In fact, CatG has been identified as a marker of airway inflammation and a predictor of disease progression in COPD [25]. Thus, small molecule or biologic inhibitors of CatG are expected to be very useful. Unfortunately, no FDA-approved inhibitor of CatG is available to date. In fact, only a few CatG inhibitors have been reported so far, such as oligopeptides, small molecules, and aptamers [13,26–28]. Of these, none have reached clinical trials [13].

Glycosaminoglycans (GAGs), especially heparin, have been reported to inhibit CatG activity [29,30]. Although recently Burster et al. state in their review that the 'characteristics of heparin to modulate the activity of CatG are controversial and might depend on the heparin concentration' [31], the promise of heparin has been that it has been known to modulate many pro-inflammatory proteases for a long time [32–36]. However, the tendency to induce bleeding and considerable heterogeneity limits its use in a majority of diseases. In this context, small sulfated molecules that mimic heparin function may represent a major avenue for discovering novel therapeutics. Whereas mimicking is typically regarded as structural in nature, we have shown over the past decade that small sulfated molecules mimic function because of the presence of multiple sulfate groups on the small scaffold.

One such small molecule, labeled as sulfated pentagalloyl glucoside (SPGG), a member of the library of non-saccharide GAG mimetics (NSGMs), was recently reported as an allosteric inhibitor of CatG [37]. Unfortunately, SPGG is also a heterogeneous mixture composed of variably-sulfated species [38]. Additionally, it inhibits human factor XIa and induces powerful blood anticoagulation [39], which could induce some bleeding risk. We reasoned that it should be possible to discover structurally-defined and homogeneous molecules that inhibit CatG with high potency and present no or minimal anticoagulation potential by screening the library of NSGMs. In this work, we screened a focused library of 30 NSGMs and identified an octasulfated **25** as a potent inhibitor of CatG (IC_{50} 53 nM). As expected, NSGM **25** was found to be an allosteric inhibitor of CatG. Interestingly, salt-dependence studies indicated that NSGM **25** utilized almost equal ionic and nonionic forces in binding to CatG, which alludes to the special role of the aromatic scaffold of these GAG mimetics. NSGM **25** did not extend human plasma clotting time in the activated partial thromboplastin time and prothrombin time assays, suggesting the strong possibility of no or minimal bleeding complications. Overall, this work presents at least one novel synthetic, homogeneous small molecule as a nanomolar allosteric inhibitor of CatG, devoid of anticoagulant properties.

2. Materials and Methods

2.1. Materials

Human CatG and chromogenic substrate for CatG (S-7388, *N*-succinyl-Ala-Ala-Pro-Phe *p*-nitroanilide) were purchased from Elastin Products Company (Owensville, MO, USA). Human plasma was obtained from George King Biomedical Inc. (Overland Park, KS, USA). Stock solutions of CatG were prepared in 20 mM tris-HCl buffer, pH 7.4, containing 0.02% Tween 80, 0.1% PEG 8000, 2.5 mM $CaCl_2$, and 100 mM NaCl. Experiments were repeated at least two times.

2.2. Chemistry

All the molecules in this study were characterized by NMR, MS, and UPLC, and reported to have purity of >95%. The synthetic schemes and spectral data of all molecules studied in this work have been previously reported [40–42].

2.3. Inhibitor Screen

Using a chromogenic substrate hydrolysis assay, compounds were screened at a concentration of 50 μM, employing a 96-well plate format. To each well of a 96-well microplate containing 88 μL of 20 mM tris buffer, which contained 100 mM NaCl, 2.5 mM $CaCl_2$, 0.1% PEG 8000, and 0.05% Tween 80, 4 μL of CatG (final concentration of 60 nM) and 5 μL of H_2O or NSGM (final concentration of 50 μM) were added. After incubating for a period of 5 min, 3 μL of CatG substrate (S-7388, final concentration of 750 μM) was added, and the residual CatG activity was obtained from the initial rate of increase of absorbance at 405 nm. The relative residual activity of CatG for each of the NSGMs, at the various concentrations, was calculated from the ratio of CatG activity in the presence and absence of NSGMs. Each compound was tested twice and compounds that showed greater than 50% inhibition of CatG were selected for IC_{50} determination.

2.4. IC_{50} Determination

A chromogenic substrate hydrolysis assay was used to determine the direct inhibition of CatG by the NSGMs, as previously reported [37]. To each well of a 96-well microplate containing 88 μL of 20 mM tris buffer, containing 100 mM NaCl, 2.5 mM $CaCl_2$, 0.1% PEG 8000, and 0.05% Tween 80, 4 μL of CatG (final concentration of 60 nM) and 5 μL of H_2O or NSGM (final concentration of 0–100 μM) were added. After incubating for a period of 5 min, 3 μL of CatG substrate (S-7388, final concentration of 750 μM) was added, and the residual CatG activity was obtained from the initial rate of increase of absorbance at 405 nm. The relative residual activity of CatG for each of the NSGMs, at the various concentrations,

was calculated from the ratio of CatG activity in the presence and absence of NSGMs. The dose dependence curve was plotted using a logistic equation (see below) in Sigmaplot version 12 to obtain the IC_{50} (potency), Hill slope (HS), and efficacy (ΔY). Here, Y is the ratio of residual CatG activity in the presence of NSGMs to that in their absence, Y_O and Y_M are the minimum and maximum values of fractional residual CatG activity, respectively, IC_{50} is the concentration of the NSGM that inhibits CatG activity by 50%, and HS is the Hill slope. $\Delta Y = Y_M - Y_O$.

$$Y = Y_O + \frac{Y_M - Y_O}{1 + 10^{(\log [I]_0 - \log IC_{50})(HS)}}$$

2.5. Michaelis–Menten Kinetics

The initial rate of the hydrolysis of CatG substrate by NSGM **25** was monitored using the linear increase in absorbance corresponding to less than 10% consumption of substrate at 37 °C in pH 7.4 20 mM tris buffer containing 100 mM NaCl, 2.5 mM $CaCl_2$, 0.1% PEG 8000, and 0.05% Tween 80, as for IC_{50} determinations. The initial rate was measured at various substrate concentrations (0–2500 μM) at fixed enzyme concentration (100 nM) and fixed inhibitor concentrations (0–200 nM). The data were analyzed using the standard Michaelis–Menten equation in Sigmaplot version 12 to determine the K_M and V_{MAX}.

2.6. Salt Dependence of NSGM **25** *Inhibition of CatG*

The direct inhibition of CatG cleavage of a chromogenic substrate was determined at 37 °C, as described above, in pH 7.4 tris buffer containing 2.5 mM $CaCl_2$, 0.1% PEG 8000, 0.05% Tween 80, and 50–200 mM NaCl. Each K_I value was calculated from the corresponding IC_{50} using the Cheng–Prusoff equation [43]. A double-log plot of the K_I against Na^+ concentration was prepared and analyzed using the equation $\log K_I = \log K_{I,NONIONIC} + Z\psi \log[Na^+]$. Here, the slope corresponds to the number of ion-pair interactions (Z) and the counterions released per negative charge upon ion binding ($\psi = 0.8$), while the intercept corresponds to the nonionic affinity ($K_{I,NONIONIC}$). The contributions of ionic and nonionic binding energies to the interactions were obtained from the slope and intercept of the plot in Excel.

2.7. Impact of NSGM **25** *on Clotting Assays*

The impacts of NSGM **25** on activated partial thromboplastin time (aPTT) and the prothrombin time (PT) of human plasma were measured employing a standard one-stage recalcification assay at 37 °C, as previously reported [44]. $CaCl_2$ and thromboplastin-D were used to initiate clotting in aPTT and PT assays, respectively, in the absence and presence of NSGM **25**, and the time to clot was recorded accordingly.

3. Results

3.1. Screening for Cathepsin G Inhibition

The library of NSGMs consisted of 30 synthetic, sulfated compounds, based on either a benzofuran or flavonoid scaffold with varying level and pattern of sulfate groups (Figure 2, Tables 1 and 2). Both benzofuran- and flavonoid-based NSGMs have been studied earlier for anticoagulant [40,45,46], antiviral [41], and antifibrinolytic activities [47]. More importantly, we reasoned that the configurational and conformational diversity afforded by these NSGMs is sufficiently broad to afford a high probability of initial hits that could later be transformed into CatG selective agents. The NSGMs were either monomers or homo-/hetero-dimers that presented a linear molecular length of ~13 to 30 Å, which is the length of a typical heparin-binding site on proteins.

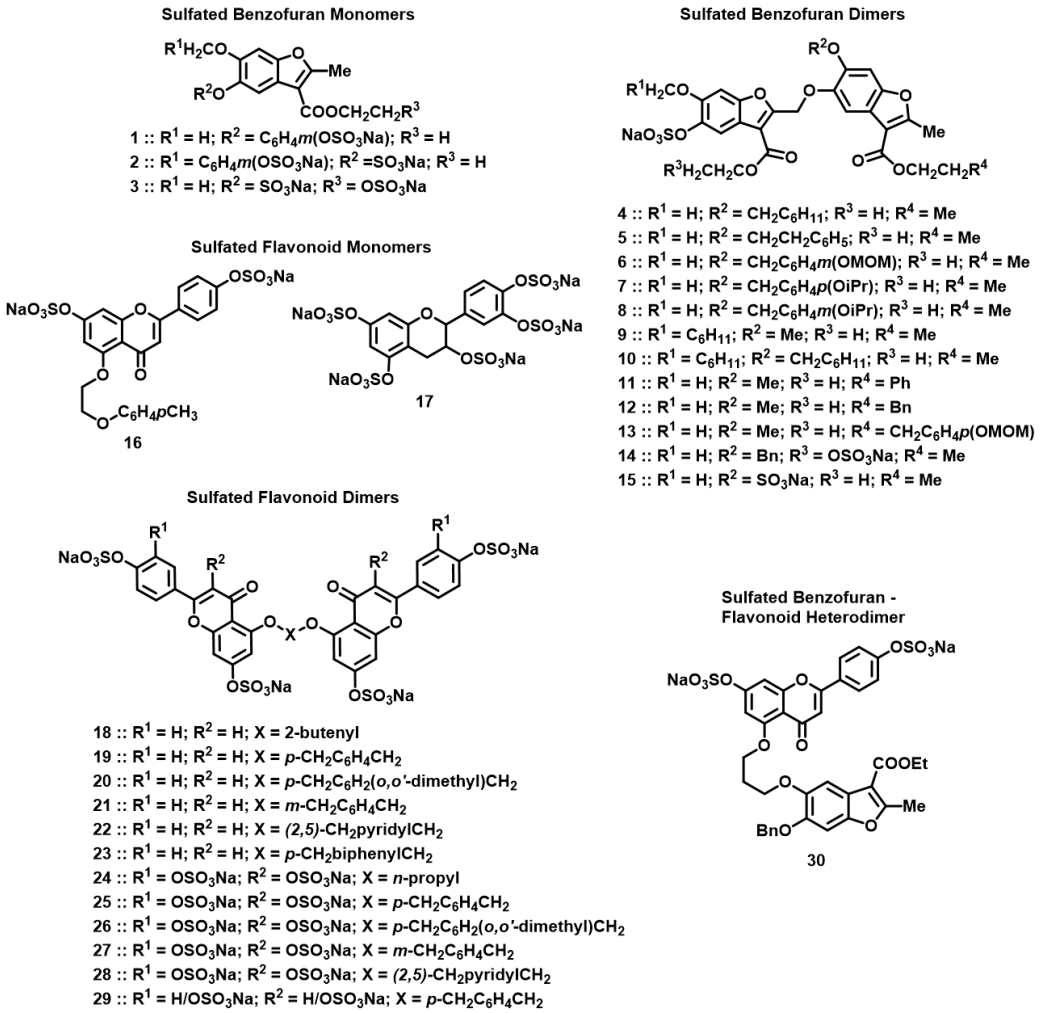

Figure 2. Chemical structures of the focused library of non-saccharide glycosaminoglycan mimetics (NSGMs). Structures studied included sulfated benzofuran monomers **1**–**3** (see Table 1 for R^1, R^2, R^3); sulfated benzofuran dimers **4**–**15** (see Table 1 for R^1, R^2, R^3 and R^4); sulfated flavonoid monomers **16** and **17**; sulfated flavonoid dimers **18**–**29** (see Table 2 for X, R^1, and R^2); and sulfated benzofuran–apigenin heterodimer **30**.

We utilized a screening strategy involving the use of a chromogenic substrate (S-7388), which had been used earlier in multiple studies [37]. We first screened the NSGMs for CatG inhibition at 50 μM in a pH 7.4 tris buffer containing 100 mM NaCl, 2.5 mM $CaCl_2$, 0.1% PEG, and 0.05% Tween 80 to quickly assess the diversity of CatG targeting [37]. Indeed, Figure 3 shows a massive structural dependence of activity, with 2–95% inhibition of CatG. Of these, monomeric NSGMs were found to be poor CatG inhibitors, with none displaying more than 50% inhibition at 50 μM. In contrast, nearly all dimeric NSGMs exhibited significant CatG inhibition (>50%). This phenomenon is similar to earlier results for many NSGM–protein systems [40,48], and correlates with the observation that longer GAGs elicit better biological responses.

Table 1. Direct Inhibition of Human CatG by Sulfated Benzofuran Molecules.

NSGM	IC_{50} (μM) [a]	ΔY (%) [b]	HS [c]
1	>50	ND	ND
2	>50	ND	ND
3	>50	ND	ND
4	48.3 ± 6.8 [d]	96 ± 6	1.3 ± 0.2
5	5.5 ± 0.8	93 ± 5	5.3 ± 1.9
6	~50	ND	ND
7	>50	ND	ND
8	27.0 ± 3.1	101 ± 5	1.7 ± 0.3
9	45.5 ± 3.3	99 ± 4	2.5 ± 0.4
10	29.0 ± 6.5	97 ± 10	1.5 ± 0.5
11	>50	ND	ND
12	19 ± 12	87 ± 4	8.6 ± 5.1
13	42.1 ± 4.2	90 ± 5	2.3 ± 0.5
14	17.3 ± 2.8	96 ± 7	1.6 ± 0.4
15	>50	ND	ND
16	126 ± 11	115 ± 4	1.9 ± 0.3
17	65 ± 13	76 ± 7	3.1 ± 1.3

[a] IC_{50} values, [b] ΔY, and HS; [c] HSs were obtained by non-linear regression of direct CatG inhibition by the NSGMs. [d] Error represents ± 1 S.E. Please refer to the Section 2.4 to review the definitions of ΔY and HS.

Table 2. Direct Inhibition of Human CatG by Sulfated Flavonoid Dimers.

NSGM	IC_{50} (μM) [a]	Δ Y (%) [b]	HS [c]
18	4.7 ± 0.7 [d]	81 ± 7	1.5 ± 0.3
19	3.3 ± 0.3	82 ± 4	3.1 ± 1.0
20	1.5 ± 0.2	89 ± 4	1.4 ± 0.2
21	10.3 ± 4.8	81 ± 7	1.3 ± 0.8
22	1.3 ± 0.2	105 ± 7	1.2 ± 0.2
23	3.4 ± 0.2	103 ± 4	4.1 ± 1.0
24	0.21 ± 0.04	94 ± 9	1.5 ± 0.5
25	0.05 ± 0.01	95 ± 7	0.7 ± 0.1
26	0.07 ± 0.01	101 ± 5	1.2 ± 0.2
27	0.15 ± 0.06	77 ± 10	0.9 ± 0.4
28	0.18 ± 0.04	77 ± 5	0.9 ± 0.2
29	0.14 ± 05	110 ± 16	1.1 ± 0.1
30	18.9 ± 2.2	87 ± 5	2.1 ± 0.5

[a] IC_{50} values, [b] ΔY, and HS; [c] HSs were obtained by non-linear regression of direct CatG inhibition by the NSGMs. [d] Error represents ± 1 S.E.

3.2. Structure–Activity Relationship (SAR)

To identify promising NSGMs, we measured the IC_{50} of 22 NSGMs that inhibited CatG by at least 50%. Figure 4 shows sigmoidal dose–response relationships for a select group of NSGMs, suggesting nearly a 1000-fold range of potencies. While sulfated benzofuran dimers **4**–**15** displayed IC_{50}s in the range of 5 to >50 μM (Table 1), sulfated flavonoid dimers presented IC_{50} in the range of 0.05–10 μM (Table 2). At first glance, this could represent a preference for the flavonoid scaffold, but such a generalization would be inaccurate because there is a vast difference in the level of sulfation between the two scaffolds. While the benzofuran dimers had only one or two sulfate moieties, the flavonoid dimers had a minimum of four sulfates. More interestingly, the level of sulfation, although necessary and important for binding to electropositive CatG (Figure 1), appears to contribute additional factors, which are described below.

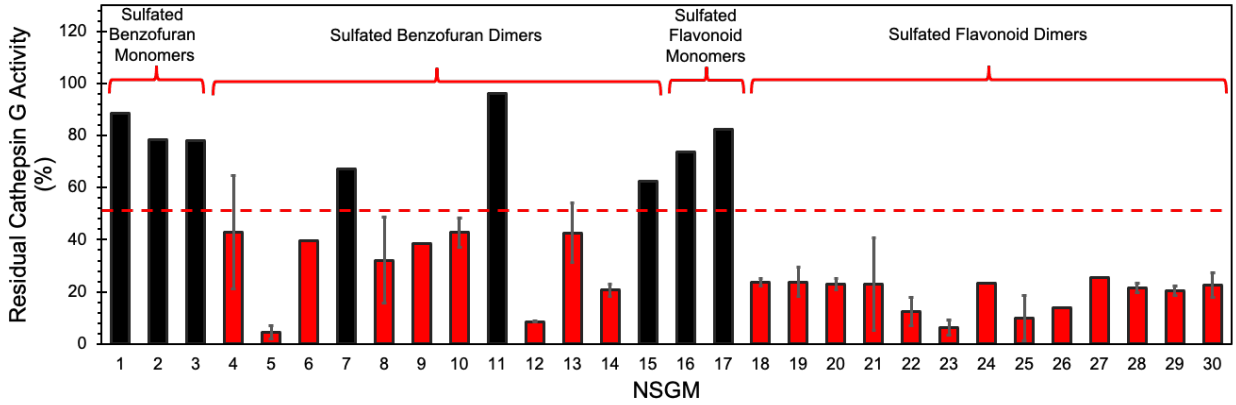

Figure 3. Screening of focused chemical library of NSGMs against CatG. CatG inhibition was measured using a chromogenic substrate hydrolysis assay in a 20 mM tris buffer, pH 7.4, containing 100 mM NaCl, 2.5 mM $CaCl_2$, 0.1% PEG, and 0.05% Tween 80 at 37 °C. Compounds were screened at 50 μM and measurements were performed at least in duplicate. Error bars represent ± 1 S.E. Red bars show compounds selected for IC_{50} determination. Black bars show compounds with <50% inhibition and identified as weak/modest inhibitors of CatG.

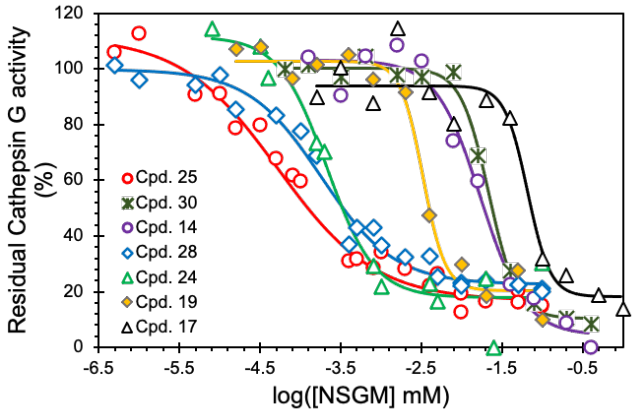

Figure 4. Representative IC_{50} profiles for CatG inhibition by NSGMs. Direct inhibition of human CatG was measured using the chromogenic substrate hydrolysis assay at pH 7.4 and 37 °C. Solid lines represent analysis using the logistic dose–response relationship (Equation (1)) to obtain the IC_{50}, ΔY%, and HS. Errors represent ± 1 S.E.

Benzofuran-based NSGMs—Although sulfated benzofuran NSGMs displayed modest IC_{50}s (5.5 to >50 μM, Table 1), interesting insights can be derived in terms of CatG recognition. CatG is a strongly basic protease with a predicted pI of 12 [49] and a predominantly electropositive surface area (Figure 1). A priori, this implies a high probability of binding to polyanionic species such as long chain GAGs. Nevertheless, mono- and di-sulfated benzofurans, consisting of hydrophobic and aromatic groups, were found to be modest inhibitors of CatG. In fact, the hydrophobic substituents, rather than the number of sulfate moieties, appeared to be more important for CatG inhibition in this series. This implies that the monosulfated benzofuran scaffold may serve as a useful fragment for conjugation with a promising hit from another screen.

This is not the first time that hydrophobic scaffolds and/or substituents of highly-sulfated NSGMs have been found to induce inhibition of serine proteases. In fact, an optimal combination of hydrophobic and anionic forces was proposed to be the basis for both affinity and selectivity of sulfated NSGMs, as described in a recent perspective [42,50,51]. More specifically, whereas sulfated benzofuran dimer **5**, having a phenethyl group at the R^2 position, displayed an IC_{50} of 5.5 μM, dimer **15**, with a sulfate group in the same position, was more than 10-fold less potent (Table 1). However, the presence of a substituted aromatic

ring in the same position, e.g., dimers **6**–**8**, resulted in at least a five-fold loss in potency. Introducing an alicyclic ring, as in dimer **4**, at the same position (R^2) led to a nine-fold loss in potency. These results suggest that the phenethyl group at the R^2 position occupies a well-defined pocket that contributes to the selectivity of binding.

The presence of a bulky hydrophobic group at the R^1 position of sulfated benzofuran dimers appears to marginally favor CatG inhibitory potency as evidenced by NSGM **10** (IC_{50} 29 μM), which was almost two-fold more potent than NSGM **4** (Table 1). Likewise, the benzyl group at the R^4 position (dimer **12**) is slightly favored over phenyl (dimer **11**) or substituted phenyl group (dimer **13**). Of note, both of these observations convey the importance of the nature of hydrophobic groups in improving potency. Interestingly, enhancing sulfation level did not offer better inhibition potential over monosulfated benzofuran dimer **5**, as evidenced by disulfated NSGMs **14** and **15**. In fact, **14** having an additional sulfate at the R^3 position was nearly three-fold less potent than dimer **5**, while NSGM **15** was essentially inactive (IC_{50} > 50 μM, Table 1).

Overall, these results for sulfated benzofuran dimers underscore the importance of the aromatic/hydrophobic groups at the R^2 position, while also emphasizing the importance of the positions, rather than the number, of sulfate groups for CatG inhibition. The SAR observed for this series of inhibitor hits suggests that appropriate modification or conjugation at the R^1 and R^3 positions may significantly increase inhibition potency. From a drug design/discovery perspective, such modifications are much easier to introduce than altering the number and position of sulfate groups.

Flavonoid-based NSGMs—This sub-library of dimers is made up of di-quercetin, quercetin–apigenin, and di-apigenin dimers with 8, 6, and 4 sulfate groups, respectively. Alternatively, this class of NSGMs was completely different from the sulfated benzofuran dimers in terms of both the scaffold as well as the level of sulfation. Table 2 lists the inhibition potencies of NSGMs **18**–**29**, which present a fairly wide range, from 0.05 to 10.3 μM. Interestingly, as a group, tetra-sulfated NSGMs, e.g., **18**–**23**, were ~50-fold less potent than octasulfated NSGMs, e.g., **24**–**28**. Alternatively, this group of NSGMs presents the conclusion that higher sulfation is better for CatG inhibition, an observation directly opposed to the results presented above for NSGMs **4**–**15** (Table 1). More specifically, comparing NSGMs with identical linkers, e.g., **25** (IC_{50} 0.05 μM) vs. **19** (IC_{50} 3.3 μM), shows a 66-fold difference between octasulfated di-quercetin NSGM and its tetra-sulfated di-apigenin counterpart.

For the di-apigenin-based NSGMs, the most potent molecule, **22** (IC_{50} 1.3 μM), had a 2,6-bis(methylene)pyridine linker (Table 2). Substitution of the linker with a 1,3-bis(methylene)benzene in NSGM **21** resulted in an eight-fold decrease in potency, possibly indicating a role for the heteroatom in binding. A change from meta- to para-substitution in the linker, i.e., **21** vs. **19**, resulted in a two-fold loss. This implies that meta to para change probably impacts the relative spatial arrangement of each monomer as well as their sulfates.

For the di-quercetin-based NSGMs, the most potent NSGM, **25** (IC_{50} 0.05 μM), had a 1,4-bis(methylene)benzene linker. Introducing methyl groups on a linker aryl ring (NSGM **26**) did not affect CatG inhibitory potency; however, a three-fold decrease in potency was observed when the linker was changed to 1,3-bis(methylene)benzene (NSGM **27**, IC_{50} 0.15 μM). This is similar to what was observed for the di-apigenin-based NSGMs (above). Contrary to the observation with di-apigenin dimer **22**, the presence of a heteroatom in the linker in di-quercetin dimer **28** had no impact on potency when compared with respective parent NSGMs (e.g., **21** and **27**). Introducing a more flexible linker induced a 4-fold loss of potency (i.e., **25** vs. **24**), and suggests a possibly-limited ability to maneuver around the linker structure.

Finally, the most convincing evidence of the importance of the linker is seen with NSGM **29**, a hexa-sulfated quercetin–apigenin heterodimer carrying a 1,4-bis(methylene)benzene linker. NSGM **29** displayed an IC_{50} of 0.14 μM, which is several-fold lower than the di-apigenin-based NSGMs (1.3–10.3 μM), but only 2.8-fold higher than the most potent di-quercetin NSGM **25** (0.05 μM). In fact, heterodimer **29** is equipotent with most di-quercetin

NSGMs, despite having two fewer sulfate groups. This implies that there is enough structural space available around the quercetin–apigenin heterodimeric scaffold for the discovery of more potent leads, if needed.

3.3. Mechanism of CatG Inhibition by NSGM **25**

GAGs typically engage proteases, especially coagulation factors, in their allosteric sites as discussed in recent articles [51,52]. Because NSGMs are known to functionally mimic GAGs, allosterism is also expected and observed, especially with regard to coagulation proteases [52]. However, structurally, NSGMs present a combination of a hydrophobic and an anionic scaffold, while GAGs are strongly anionic, which may induce different binding sites and/or geometries for some proteins. In fact, one example of this phenomenon has already been documented. A monosulfated benzofuran-based NSGM inhibited thrombin by binding in a locale different from that of a heparan sulfate oligosaccharide [53]. Thus, it is important to assess the mechanism of inhibition induced by NSGMs, especially the most promising molecules, for every target protease. The most promising molecule in this work was found to be NSGM **25** (IC_{50} = 50 nM), which is the reason mechanistic studies were performed for this representative inhibitor.

We employed Michaelis–Menten kinetic studies to define the mechanism of CatG inhibition by NSGM **25** at pH 7.4 and 37 °C (Figure 5). In the absence of **25**, the K_M for the substrate was 2.26 ± 0.28 mM. As the concentration of **25** increased from 50 to 400 nM, the K_M decreased consistently and reached a value of 0.8 ± 0.3 mM (Table 3). Similarly, there was a corresponding decrease in the V_{MAX} from 70 ± 6 to 12 ± 2 mAu/min. The simultaneous reductions in both K_M and V_{MAX} suggest an uncompetitive inhibition mechanism, a type of allosteric inhibition where the inhibitor preferentially binds only to the substrate-bound protease to bring about inhibition.

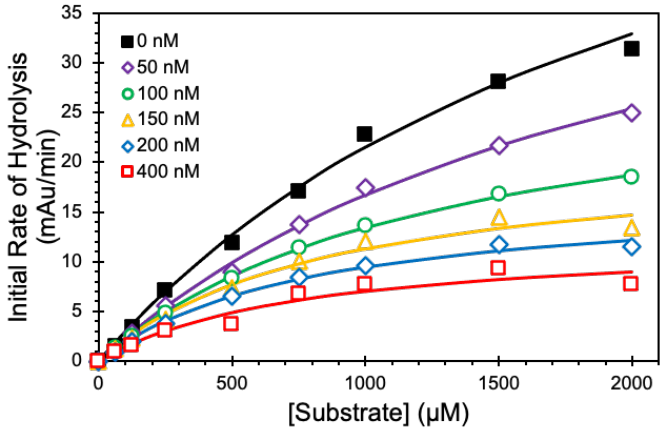

Figure 5. Kinetics of inhibition of 60 nM CatG by NSGM **25**. Michaelis–Menten kinetics of CatG hydrolysis of chromogenic substrate (S-7388) in the presence of NSGM **25**. Experiments were performed at 37 °C in 20 mM tris buffer, pH 7.4. Solid lines represent nonlinear regression analysis of the data using the standard Michaelis-Menten to calculate K_M and V_{MAX}.

3.4. Salt-Dependence of CatG Inhibition in the Presence of NSGM **25**

A fundamental point being advanced in NSGM-based mimicry is the presumed increase in hydrophobic forces contributing to binding affinity. As is well-recognized, heparin and other GAGs utilize primarily electrostatic forces in binding to proteins [54]. Only when the contribution of nonionic forces, e.g., van der Waals, and/or directional ionic forces, e.g., hydrogen bonding (H-bonding), is high enough do GAGs exhibit a high level of selectivity. This is exemplified by the classic case of antithrombin binding to heparin, which exhibits nearly 60% nonionic binding energy [55,56]. The resolution of overall binding energy into ionic and nonionic contributions is typically achieved by performing affinity measurements as a function of the ionic strength of the buffer. According to the

protein–polyelectrolyte theory [57], the two contributions can be resolved from a double-log plot of binding affinity against the Na^+ concentration, as defined by the equation log K_I = log $K_{I,NONIONIC}$ + Zψ × log [Na^+], where Z represents the number of salt interactions, and ψ is the proportion of Na^+ released per anion upon ligand binding and is equal to 0.8 for heparin [55].

Table 3. Michaelis–Menten Kinetics of CatG Hydrolysis of Chromogenic Substrate (S-7388) in the Presence of NSGM **25** [a].

[NSGM 25] (nM)	K_M (mM)	V_{MAX} (mAu/min)
0	2.26 ± 0.28 [b]	70.0 ± 5.5
50	2.18 ± 0.27	52.9 ± 4.1
100	1.31 ± 0.06	31.0 ± 0.8
150	0.87 ± 0.2	21.1 ± 2.1
200	0.80 ± 0.11	17.0 ± 1.0
400	0.77 ± 0.30	12.4 ± 2.1

[a] K_M and V_{MAX} values were measured as described in the experimental section. mAU indicates milliabsorbance units. [b] Error represents ± 1 S.E.

To resolve these two types of contributing forces, we measured the IC_{50} of NSGM **25** at pH 7.4 and 37 °C as a function of the ionic strength of the buffer (Figure 6A). The dose dependence profiles clearly show a loss in potency, as expected. In fact, the IC_{50} values increased from 0.043 ± 0.01 μM to 3.42 ± 0.52 μM as NaCl concentration was increased from 50 mM to 200 mM (Table 4). This represents a substantial loss of ~80-fold in inhibition potency, and demonstrates that ionic forces are important to the CatG–NSGM **25** system.

Table 4. Salt-Dependence of CatG Inhibition by NSGM **25**.

[NaCl]	IC_{50} (nM) [a]	ΔY (%) [b]	HS [c]	K_I (nM) [d]
50	42.7 ± 10	87.7 ± 7.3 [b]	1.3 ± 0.4	10.9 ± 3.9
100	52.6 ± 12.2	94.9 ± 17.9	0.7 ± 0.1	19.2 ± 5.3
150	318.6 ± 44.5	74.4 ± 2.9	1.6 ± 0.3	148 ± 54
200	3453 ± 517	73.2 ± 4.9	2.0 ± 0.5	1671 ± 480

[a] IC_{50} values, [b] ΔY, and HS; [c] HS were obtained by non-linear regression of direct CatG inhibition by NSGM **25**. [d] Calculated using Cheng–Prusoff equation [54].

The measured IC_{50}s of our allosteric inhibitors are distinct from inhibition constants K_I, which are thermodynamic constants. Cheng and Prusoff provided a mathematical foundation for the transformation of IC_{50}s into K_Is for uncompetitive inhibitors. In their formulation, K_I is equal to IC_{50} × [S]/(K_M + [S]) [43], which is directly applicable to our study. Thus, it becomes possible to utilize the linear double-log analysis described above for our NSGM **25**, which is an uncompetitive inhibitor. Figure 6B shows the double-log plot of K_I versus Na^+ concentration, where the inhibition constants were calculated from the observed IC_{50} values. Linear regression yielded a slope of 2.94 and an intercept of −4.32 (Table 5). Whereas the former corresponds to an ionic binding energy of 4.88 kcal/mol at 37 °C and 100 mM salt, the latter yields a nonionic binding energy of 6.12 kcal/mol. These results show that the NSGM **25** interaction with CatG is driven by both electrostatic (~44%) and nonionic forces (~56%). Such important roles of two forces have not been observed earlier. More importantly, the higher nonionic component bodes well for the discovery of second-generation inhibitors with higher selectivity.

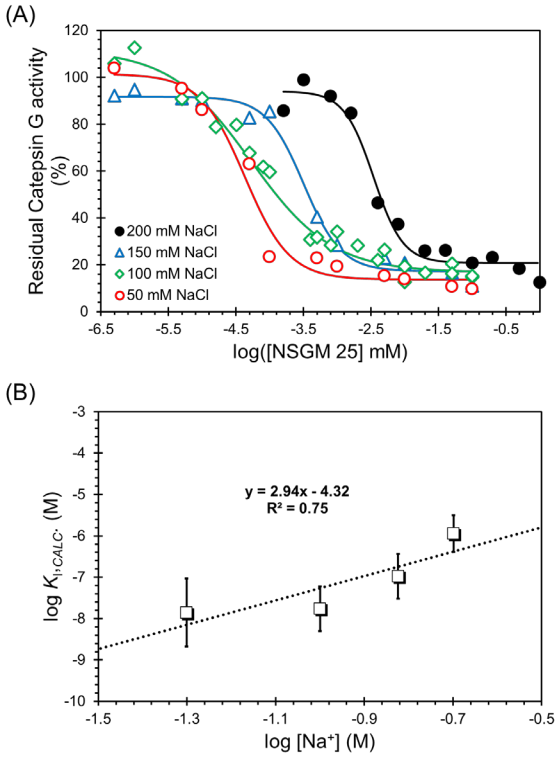

Figure 6. Salt dependence of CatG inhibition by NSGM **25**. (**A**) Salt-dependent direct inhibition of CatG by NSGM **25**. Data were obtained using substrate S-7388 in a chromogenic substrate hydrolysis assay. Solid lines represent sigmoidal dose–response analysis (Equation (1)) of the data to obtain IC_{50}, ΔY%, and HS. Errors represent ± 1 S.E. (**B**) A double-log plot of the K_I calculated using Cheng–Rusoff equation for uncompetitive inhibition against the concentration of salt. Solid line shows linear analysis to obtain the intercept (log $K_{D,NONIONIC}$) and slope (Z × ψ) (see Section 2.6), from which proportions of nonionic and ionic binding energies were derived.

Table 5. Calculated energies of binding of CatG and NSGM **25**.

Slope	Intercept	$K_{I,NON\text{-}IONIC}$ (μM)	$\Delta G_{NON\text{-}IONIC}$ (kcal/mol)	$\Delta G_{NON\text{-}IONIC}$ (%)	ΔG_{IONIC} (%)
2.94	−4.32	158.5	6.12	55.6	44.4

Slope and intercept were calculated from linear regression analysis of log K_I versus log[Na^+] using the equation log K_I = log $K_{I,NONIONIC}$ + Zψ log [Na^+] [53].

3.5. Impact of NSGM **25** *on Human Plasma Clotting*

Considering that NSGMs are functional mimetics of heparins, they have the potential to impact blood clotting by interfering with the activity of heparin-binding coagulation enzymes. For NSGM **25** to be useful as an anti-CatG agent in inflammatory conditions, it is important that it possesses a minimal risk of bleeding. In a previous study, we had reported that the inhibitory potencies of NSGM **25** against thrombin, factor Xa, factor XIa, factor IXa, and factor XIIa were poor (>150 μM) [47]. This implied a rather weak anticoagulant activity. However, a key test of clotting risk is the impact putative anticoagulants have on human plasma. To evaluate this, we measured the effect of NSGM **25** on activated partial thromboplastin time (aPTT) and prothrombin time (PT), two in vitro tests that are routinely used to assess anticoagulant potency [58]. Figure 7 shows the effect of specific concentrations of NSGM **25** and the clinically-approved anticoagulants unfractionated heparin (UFH), argatroban, and rivaroxaban on clotting time in the aPTT and PT assays. NSGM **25** did not impact either aPTT or PT at a concentration as high as 1 mM, which greatly exceeds its in vitro IC_{50} against CatG. In contrast, the clinically-approved anticoagulants doubled both the aPTT and PT at sub-micromolar concentrations (Table 6). Thus, NSGM **25**

is not expected to present a high risk of bleeding, a significant advantage over current anticoagulants. Advanced studies will be needed to study the bleeding propensity of NSGM **25** in vivo.

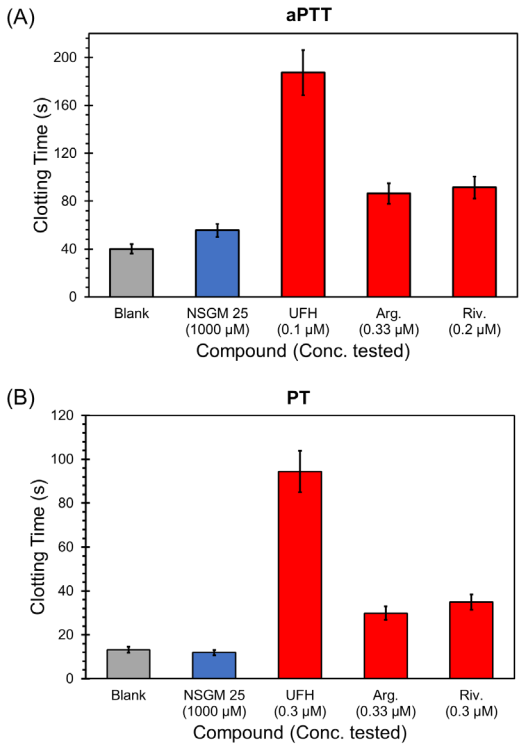

Figure 7. Impact of specific concentrations of NSGM 25 (blue bar) and the clinically-approved anticoagulants unfractionated heparin, argatroban, and rivaroxaban (red bars) on (**A**) activated partial thromboplastin time (aPTT) and (**B**) prothrombin time (PT). Grey bars are control experiments in which only buffer is used to measure clotting times.

Table 6. Impact of NSGM **25** on aPTT and PT [a].

Sample	aPTT (EC_{2X}) (μM)	PT (EC_{2X}) (μM)
NSGM **25**	>1000	>1000
UFH	0.045	0.170
Argatroban	0.34	0.36
Rivaroxaban	0.12	0.15

[a] Concentrations of molecules required to double the aPTT or the PT of pooled human plasma.

4. Discussion

We pursued NSGM inhibition of CatG because of its importance in several inflammatory diseases, which has been challenging to fully understand because of the paucity of synthetic small molecule inhibitors, which may serve as high-quality chemical probes and eventually lead to therapeutics. In fact, it has been challenging to decipher the exact roles of different NSPs contributing to the protease–antiprotease balance, and high-quality chemical probes of CatG may aid in understanding the biology better. Nevertheless, in the context of therapy, it may be advantageous to also discover pan-protease inhibitor(s) that target CatG together with other pro-inflammatory proteases, e.g., HNE, PR3, and NSP4. One route to achieve this is to explore sulfated NSGMs because each of these proteases is known to bind to highly anionic biopolymers, e.g., GAGs and/or DNA [27,29,59–61].

In this study, we have shown that several structurally-defined, homogeneous NSGMs hold considerable promise as chemical biology probes of CatG, and may serve as early leads for therapeutics development. More specifically, the sulfated flavonoid class of NSGMs is

especially promising because it presents two molecules with 53 nM (NSGM **25**) and 70 nM (NSGM **26**) inhibition potency. Discovery of such high-potency protease inhibitors in the first screen itself is a major achievement, when first attempts against other serine proteases, e.g., thrombin, factor Xa, factor XIa, etc., are considered [51,52]. This bodes well for further optimization of NSGM structure for potency as well as selectivity.

Although it may appear that sulfated benzofuran-based NSGMs are not worthy of further studies because of their moderate IC_{50}s, these molecules may serve a very important function. Analysis of the drivers of their inhibition potency revealed that hydrophobicity and placement of hydrophobic groups were more important than the number of sulfate groups. In contrast, the sulfated flavonoid-based NSGMs emphasized the latter to be more important. Such divergent drivers of affinity could arise from different sites of binding on CatG. If so, it may be possible to use a fragment-based structural biology approach to develop a heterodimer from a sulfated benzofuran and sulfated flavonoid, thereby enhancing affinity as well as selectivity.

Michaelis–Menten studies revealed that NSGM **25** utilizes an uncompetitive inhibition mechanism. The simultaneous reduction in both K_M and V_{MAX} implies that **25** prefers the enzyme–substrate complex rather than the enzyme alone. This is an uncommon mechanism of inhibition because the majority of NSGMs studied to date have exhibited non-competitive inhibition mechanism [52]. Mechanistically, this phenomenon is extremely interesting because it implies that the binding of NSGM **25** in its allosteric site makes the enzyme recognize its substrate better, while at the same time not allowing it to perform its catalytic function. Structurally, it implies that the catalytic triad present in the active site is disrupted upon inhibitor complexation, but the other residues of the active site hold on to the substrate better.

The salt dependence studies provide another window into the recognition of NSGM **25** by CatG. These experiments show that NSGM **25** binding to CatG is driven by both electrostatic (~44%) and nonionic forces (~56%). The relatively high nonionic component of binding energy is interesting considering that electrostatics dominate the overall surface area of CatG. Because nonionic binding energy may arise from H-bonding, which is highly directional, and/or van der Waals forces, which have to be structurally complementary, the CatG–NSGM **25** interaction is expected to exhibit significant structural selectivity.

There are several advantages of pursuing NSGM **25** for further development as a probe and/or therapeutic agent. First, in contrast to GAGs and heparin, it is a small, homogeneous compound that can be obtained fairly readily via synthetic means using commercially-available raw materials [47]. NSGM **25** also works via an allosteric process and, because allosteric sites on proteins are less conserved than orthosteric sites, there is a reduced possibility of off-target effects. This is also evident in its inability to inhibit coagulation proteases and impact on plasma clotting. More importantly, previous studies with NSGM **25** show its excellent inhibition of HNE (IC_{50} ~230 nM) [62] and moderate inhibition of human plasmin (IC_{50} ~6.3 μM) [47], both of which are known to be pro-inflammatory [63–65]. While HNE potentiates inflammation via mechanisms similar to CatG [44], plasmin enhances multiple pro-inflammatory responses, including the generation of pro-inflammatory fibrin degradation products, activation of the complement, and activation of matrix metalloproteinases [66]. Thus, NSGM **25**'s multiple inflammatory proteases activity, in the absence of impact on coagulation proteases, makes it a very promising inhibitor for further development. As with any such early study, this promise should always be balanced by cross-checking reactivities with other related proteases, such as those of the complement cascade, which may or may not interfere with the functions of such novel probes.

Author Contributions: Project conceptualization (D.K.A., U.R.D., R.A.A.-H. and R.M.F.); chemical synthesis (D.K.A. and S.M.), IC_{50} determinations and Michaelis–Menten studies (D.K.A., V.R.P. and E.K.L.); plasma clotting assays (S.R.D. and R.M.F.); first draft of manuscript (D.K.A.); revision of manuscript (U.R.D., R.A.A.-H., R.M.F. and D.K.A.). All authors have read and agreed to the published version of the manuscript.

Funding: This work was supported by NIH-NHLBI grant K99 HL161423 (to D.K.A.) and NIH grants P01 HL151333 & R61 HL161813 (to U.R.D.)

Institutional Review Board Statement: Not applicable.

Informed Consent Statement: Not applicable.

Data Availability Statement: Not applicable.

Acknowledgments: We thank the Washington and Lee University's Allen Grant and Livesay Grant for the support of summer research of V.R.P., E.K.L. and S.M. at Virginia Commonwealth University under the mentorship of the corresponding author.

Conflicts of Interest: The authors declare no conflict of interest.

References

1. Stapels, D.A.C.; Geisbrecht, B.V.; Rooijakkers, S.H.M. Neutrophil Serine Proteases in Antibacterial Defense. *Curr. Opin. Microbiol.* **2015**, *23*, 42–48. [CrossRef]
2. Korkmaz, B.; Horwitz, M.S.; Jenne, D.E.; Gauthier, F. Neutrophil Elastase, Proteinase 3, and Cathepsin Gas Therapeutic Targets in Human Diseases. *Pharmacol. Rev.* **2010**, *62*, 726–759. [CrossRef]
3. Hof, P.; Mayr, I.; Huber, R.; Korzus, E.; Potempa, J.; Travis, J.; Powers, J.C.; Bode, W. The 1.8 Å Crystal Structure of Human Cathepsin G in Complex with Suc-Val-Pro-Phe(P)-(OPh)2: A Janus-Faced Proteinase with Two Opposite Specificities. *EMBO J.* **1996**, *15*, 5481–5491. [CrossRef]
4. Helske, S.; Syväranta, S.; Kupari, M.; Lappalainen, J.; Laine, M.; Lommi, J.; Turto, H.; Mäyränpää, M.; Werkkala, K.; Kovanen, P.T.; et al. Possible Role for Mast Cell-Derived Cathepsin G in the Adverse Remodelling of Stenotic Aortic Valves. *Eur. Heart J.* **2006**, *27*, 1495–1504. [CrossRef]
5. Tani, K.; Murphy, W.J.; Chertov, O.; Oppenheim, J.J.; Wang, J.M. The Neutrophil Granule Protein Cathepsin G Activates Murine T Lymphocytes and Upregulates Antigen-Specific Ig Production in Mice. *Biochem. Biophys. Res. Commun.* **2001**, *282*, 971–976. [CrossRef]
6. LaRosa, C.A.; Rohrer, M.J.; Benoit, S.E.; Rodino, L.J.; Barnard, M.R.; Michelson, A.D. Human Neutrophil Cathepsin G Is a Potent Platelet Activator. *J. Vasc. Surg.* **1994**, *19*, 306–318. [CrossRef]
7. Rykl, J.; Thiemann, J.; Kurzawski, S.; Pohl, T.; Gobom, J.; Zidek, W.; Schlüter, H. Renal Cathepsin G and Angiotensin II Generation. *J. Hypertens.* **2006**, *24*, 1797–1807. [CrossRef]
8. Shamamian, P.; Schwartz, J.D.; Pocock, B.J.Z.; Monea, S.; Whiting, D.; Marcus, S.G.; Mignatti, P. Activation of Progelatinase A (MMP-2) by Neutrophil Elastase, Cathepsin G, and Proteinase-3: A Role for Inflammatory Cells in Tumor Invasion and Angiogenesis. *J. Cell. Physiol.* **2001**, *189*, 197–206. [CrossRef]
9. Wilson, T.J.; Nannuru, K.C.; Singh, R.K. Cathepsin G-Mediated Activation of pro-Matrix Metalloproteinase 9 at the Tumor-Bone Interface Promotes Transforming Growth Factor-β Signaling and Bone Destruction. *Mol. Cancer Res.* **2009**, *7*, 1224–1233. [CrossRef]
10. Son, E.D.; Kim, H.; Choi, H.; Lee, S.H.; Lee, J.Y.; Kim, S.; Closs, B.; Lee, S.; Chung, J.H.; Hwang, J.S. Cathepsin G Increases MMP Expression in Normal Human Fibroblasts through Fibronectin Fragmentation, and Induces the Conversion of ProMMP-1 to Active MMP-1. *J. Dermatol. Sci.* **2009**, *53*, 150–152. [CrossRef]
11. Jun, H.K.; Jung, Y.J.; Ji, S.; An, S.J.; Choi, B.K. Caspase-4 Activation by a Bacterial Surface Protein Is Mediated by Cathepsin G in Human Gingival Fibroblasts. *Cell Death Differ.* **2018**, *25*, 380–391. [CrossRef] [PubMed]
12. Fu, Z.; Thorpe, M.; Alemayehu, R.; Roy, A.; Kervinen, J.; de Garavilla, L.; Åbrink, M.; Hellman, L. Highly Selective Cleavage of Cytokines and Chemokines by the Human Mast Cell Chymase and Neutrophil Cathepsin G. *J. Immunol.* **2017**, *198*, 1474–1483. [CrossRef]
13. Kosikowska, P.; Lesner, A. Inhibitors of Cathepsin G: A Patent Review (2005 to Present). *Expert Opin. Ther. Pat.* **2013**, *23*, 1611–1624. [CrossRef] [PubMed]
14. Wiedow, O.; Meyer-Hoffert, U. Neutrophil Serine Proteases: Potential Key Regulators of Cell Signalling during Inflammation. *J. Intern. Med.* **2005**, *257*, 319–328. [CrossRef] [PubMed]
15. Pham, C.T.N. Neutrophil Serine Proteases Fine-Tune the Inflammatory Response. *Int. J. Biochem. Cell Biol.* **2008**, *40*, 1317–1333. [CrossRef] [PubMed]
16. Pham, C.T.N. Neutrophil Serine Proteases: Specific Regulators of Inflammation. *Nat. Rev. Immunol.* **2006**, *6*, 541–550. [CrossRef]
17. Meyer-Hoffert, U.; Wiedow, O. Neutrophil Serine Proteases: Mediators of Innate Immune Responses. *Curr. Opin. Hematol.* **2011**, *18*, 19–24. [CrossRef]
18. Miyata, J.; Tani, K.; Sato, K.; Otsuka, S.; Urata, T.; Lkhagvaa, B.; Furukawa, C.; Sano, N.; Sone, S. Cathepsin G: The Significance in Rheumatoid Arthritis as a Monocyte Chemoattractant. *Rheumatol. Int.* **2007**, *27*, 375–382. [CrossRef]
19. Krasavin, M.Y.; Gureev, M.A.; Garabadzhiu, A.V.; Pashkin, A.Y.; Zhukov, A.S.; Khairutdinov, V.R.; Samtsov, A.V.; Shvets, V.I. Inhibition of Neutrophil Elastase and Cathepsin G As a New Approach to the Treatment of Psoriasis: From Fundamental Biology to Development of New Target-Specific Drugs. *Dokl. Biochem. Biophys.* **2019**, *487*, 272–276. [CrossRef]

20. Guo, J.; Tu, J.; Hu, Y.; Song, G.; Yin, Z. Cathepsin G Cleaves and Activates IL-36γ and Promotes the Inflammation of Psoriasis. *Drug Des. Dev. Ther.* **2019**, *13*, 581–588. [CrossRef]
21. Gudmann, N.S.; Manon-Jensen, T.; Sand, J.M.B.; Diefenbach, C.; Sun, S.; Danielsen, A.; Karsdal, M.A.; Leeming, D.J. Lung Tissue Destruction by Proteinase 3 and Cathepsin G Mediated Elastin Degradation Is Elevated in Chronic Obstructive Pulmonary Disease. *Biochem. Biophys. Res. Commun.* **2018**, *503*, 1284–1290. [CrossRef] [PubMed]
22. Pandey, K.C.; De, S.; Mishra, P.K. Role of Proteases in Chronic Obstructive Pulmonary Disease. *Front. Pharmacol.* **2017**, *8*, 512. [CrossRef] [PubMed]
23. Guyot, N.; Wartelle, J.; Malleret, L.; Todorov, A.A.; Devouassoux, G.; Pacheco, Y.; Jenne, D.E.; Belaaouaj, A. Unopposed Cathepsin G, Neutrophil Elastase, and Proteinase 3 Cause Severe Lung Damage and Emphysema. *Am. J. Pathol.* **2014**, *184*, 2197–2210. [CrossRef]
24. Suter, S.; Schaad, U.B.; Morgenthaler, J.J.; Chevallier, I.; Schnebli, H.P. Fibronectin-Cleaving Activity in Bronchial Secretions of Patients with Cystic Fibrosis. *J. Infect. Dis.* **1988**, *158*, 89–100. [CrossRef] [PubMed]
25. Guerra, M.; Frey, D.; Hagner, M.; Dittrich, S.; Paulsen, M.; Mall, M.A.; Schultz, C. Cathepsin G Activity as a New Marker for Detecting Airway Inflammation by Microscopy and Flow Cytometry. *ACS Cent. Sci.* **2019**, *5*, 539–548. [CrossRef] [PubMed]
26. Swedberg, J.E.; Li, C.Y.; de Veer, S.J.; Wang, C.K.; Craik, D.J. Design of Potent and Selective Cathepsin G Inhibitors Based on the Sunflower Trypsin Inhibitor-1 Scaffold. *J. Med. Chem.* **2017**, *60*, 658–667. [CrossRef] [PubMed]
27. Craciun, I.; Fenner, A.M.; Kerns, R.J. N-Arylacyl O-Sulfonated Aminoglycosides as Novel Inhibitors of Human Neutrophil Elastase, Cathepsin G and Proteinase 3. *Glycobiology* **2016**, *26*, 701–709. [CrossRef]
28. Sieńczyk, M.; Lesner, A.; Wysocka, M.; Łegowska, A.; Pietrusewicz, E.; Rolka, K.; Oleksyszyn, J. New Potent Cathepsin G Phosphonate Inhibitors. *Bioorg. Med. Chem.* **2008**, *16*, 8863–8867. [CrossRef]
29. Sissi, C.; Lucatello, L.; Naggi, A.; Torri, G.; Palumbo, M. Interactions of Low-Molecular-Weight Semi-Synthetic Sulfated Heparins with Human Leukocyte Elastase and Human Cathepsin G. *Biochem. Pharmacol.* **2006**, *71*, 287–293. [CrossRef]
30. Ledoux, D.; Merciris, D.; Barritault, D.; Caruelle, J.P. Heparin-like Dextran Derivatives as Well as Glycosaminoglycans Inhibit the Enzymatic Activity of Human Cathepsin G. *FEBS Lett.* **2003**, *537*, 23–29. [CrossRef]
31. Burster, T.; Mustafa, Z.; Myrzakhmetova, D.; Zhanapiya, A.; Zimecki, M. Hindrance of the proteolytic activity of neutrophil-derived serine proteases by serine protease inhibitors as a management of cardiovascular diseases and chronic inflammation. *Front. Chem.* **2021**, *9*, 784003. [CrossRef] [PubMed]
32. Morla, S. Glycosaminoglycans and Glycosaminoglycan Mimetics in Cancer and Inflammation. *Int. J. Mol. Sci.* **2019**, *20*, 1963. [CrossRef]
33. Voynow, J.A.; Zheng, S.; Kummarapurugu, A.B. Glycosaminoglycans as Multifunctional Anti-Elastase and Anti-Inflammatory Drugs in Cystic Fibrosis Lung Disease. *Front. Pharmacol.* **2020**, *11*, 1011. [CrossRef] [PubMed]
34. Kummarapurugu, A.B.; Afosah, D.K.; Sankaranarayanan, N.V.; Gangji, R.N.; Zheng, S.; Kennedy, T.; Rubin, B.K.; Voynow, J.A.; Desai, U.R. Molecular Principles for Heparin Oligosaccharide-Based Inhibition of Neutrophil Elastase in Cystic Fibrosis. *J. Biol. Chem.* **2018**, *293*, 12480–12490. [CrossRef] [PubMed]
35. Casu, B.; Naggi, A.; Torri, G. Heparin-Derived Heparan Sulfate Mimics to Modulate Heparan Sulfate-Protein Interaction in Inflammation and Cancer. *Matrix Biol.* **2010**, *29*, 442–452. [CrossRef]
36. Griffin, K.L.; Fischer, B.M.; Kummarapurugu, A.B.; Zheng, S.; Kennedy, T.P.; Rao, N.V.; Foster, W.M.; Voynow, J.A. 2-O, 3-O-Desulfated Heparin Inhibits Neutrophil Elastase-Induced HMGB-1 Secretion and Airway Inflammation. *Am. J. Respir. Cell Mol. Biol.* **2014**, *50*, 684–689. [CrossRef] [PubMed]
37. Al-Horani, R.A.; Afosah, D.K.; Kar, S.; Aliter, K.F.; Mottamal, M. Sulfated Penta-Galloyl Glucopyranoside (SPGG) Is Glycosaminoglycan Mimetic Allosteric Inhibitor of Cathepsin G. *RPS Pharm. Pharmacol. Rep.* **2023**, *2*, rqad001. [CrossRef]
38. Al-Horani, R.A.; Desai, U.R. Designing Allosteric Inhibitors of Factor XIa. Lessons from the Interactions of Sulfated Pentagalloylglucopyranosides. *J. Med. Chem.* **2014**, *57*, 4805–4818. [CrossRef]
39. Al-Horani, R.A.; Ponnusamy, P.; Mehta, A.Y.; Gailani, D.; Desai, U.R. Sulfated Pentagalloylglucoside Is a Potent, Allosteric, and Selective Inhibitor of Factor XIa. *J. Med. Chem.* **2013**, *56*, 867–878. [CrossRef]
40. Afosah, D.K.; Verespy, S.; Al-Horani, R.A.; Boothello, R.S.; Karuturi, R.; Desai, U.R. A Small Group of Sulfated Benzofurans Induces Steady-State Submaximal Inhibition of Thrombin. *Bioorg. Med. Chem. Lett.* **2018**, *28*, 1101–1105. [CrossRef]
41. Sidhu, P.S.; Liang, A.; Mehta, A.Y.; Abdel Aziz, M.H.; Zhou, Q.; Desai, U.R. Rational Design of Potent, Small, Synthetic Allosteric Inhibitors of Thrombin. *J. Med. Chem.* **2011**, *54*, 5522–5531. [CrossRef]
42. Abdel Aziz, M.H.; Sidhu, P.S.; Liang, A.; Kim, J.Y.; Mosier, P.D.; Zhou, Q.; Farrell, D.H.; Desai, U.R. Designing Allosteric Regulators of Thrombin. Monosulfated Benzofuran Dimers Selectively Interact with Arg173 of Exosite 2 to Induce Inhibition. *J. Med. Chem.* **2012**, *55*, 6888–6897. [CrossRef] [PubMed]
43. Gangji, R.N.; Sankaranarayanan, N.V.; Elste, J.; Al-Horani, R.A.; Afosah, D.K.; Joshi, R.; Tiwari, V.; Desai, U.R. Inhibition of Herpes Simplex Virus-1 Entry into Human Cells by Nonsaccharide Glycosaminoglycan Mimetics. *ACS Med. Chem. Lett.* **2018**, *9*, 797–802. [CrossRef] [PubMed]
44. Afosah, D.K.; Al-Horani, R.A.; Sankaranarayanan, N.V.; Desai, U.R. Potent, Selective, Allosteric Inhibition of Human Plasmin by Sulfa Non-Saccharide Glycosaminoglycan Mimetics. *J. Med. Chem.* **2017**, *60*, 641–657. [CrossRef] [PubMed]
45. Al-Horani, R.A.; Karuturi, R.; White, D.T.; Desai, U.R. Plasmin Regulation through Allosteric, Sulfated, Small Molecules. *Molecules* **2015**, *20*, 608–624. [CrossRef]

46. Salvesen, G.; Cathespin, G. *Handbook of Proteolytic Enzymes*, 3rd ed.; Rawlings, N.D., Salvesen, G., Eds.; Academic Press: Oxford, UK, 2013; Volume 1–3, pp. 2661–2666. [CrossRef]
47. Hileman, R.E.; Jennings, R.N.; Linhardt, R.J. Thermodynamic Analysis of the Heparin Interaction with a Basic Cyclic Peptide Using Isothermal Titration Calorimetry. *Biochemistry* **1998**, *37*, 15231–15237. [CrossRef]
48. Henry, B.L.; Connell, J.; Liang, A.; Krishnasamy, C.; Desai, U.R. Interaction of Antithrombin with Sulfated, Low Molecular Weight Lignins. Opportunities for Potent, Selective Modulation of Antithrombin Function. *J. Biol. Chem.* **2009**, *284*, 20897–20908. [CrossRef]
49. Abdelfadiel, E.I.; Gunta, R.; Villuri, B.K.; Afosah, D.K.; Sankaranarayanan, N.V.; Desai, U.R. Designing Smaller, Synthetic, Functional Mimetics of Sulfated Glycosaminoglycans as Allosteric Modulators of Coagulation Factors. *J. Med. Chem.* **2023**, *6*, 4503–4531. [CrossRef]
50. Afosah, D.K.; Al-Horani, R.A. Sulfated Non-Saccharide Glycosaminoglycan Mimetics as Novel Drug Discovery Platform for Various Pathologies. *Curr. Med. Chem.* **2018**, *27*, 3412–3447. [CrossRef]
51. Gandhi, N.S.; Mancera, R.L. The Structure of Glycosaminoglycans and Their Interactions with Proteins. *Chem. Biol. Drug Des.* **2008**, *72*, 455–482. [CrossRef]
52. Olson, S.T.; Bjork, I. Predominant Contribution of Surface Approximation to the Mechanism of Heparin Acceleration of the Antithrombin-Thrombin Reaction: Elucidation from Salt Concentration Effects. *J. Biol. Chem.* **1991**, *266*, 6353–6364. [CrossRef] [PubMed]
53. Jairajpuri, M.A.; Lu, A.; Desai, U.; Olson, S.T.; Bjork, I.; Bock, S.C. Antithrombin III Phenylalanines 122 and 121 Contribute to Its High Affinity for Heparin and Its Conformational Activation. *J. Biol. Chem.* **2003**, *278*, 15941–15950. [CrossRef] [PubMed]
54. Desai, U.R.; Petitou, M.; Björk, I.; Olson, S.T. Mechanism of Heparin Activation of Antithrombin. Role of Individual Residues of the Pentasaccharide Activating Sequence in the Recognition of Native and Activated States of Antithrombin. *J. Biol. Chem.* **1998**, *273*, 7478–7487. [CrossRef]
55. Cheng, Y.-C.; Prusoff, W.H. Relationship between the Inhibition Constant (K_1) and the Concentration of Inhibitor Which Causes 50 per Cent Inhibition (I_{50}) of an Enzymatic Reaction. *Biochem. Pharmacol.* **1973**, *22*, 3099–3108. [CrossRef] [PubMed]
56. Favaloro, E.J.; Lippi, G.; Koutts, J. Laboratory Testing of Anticoagulants: The Present and the Future. *Pathology* **2011**, *43*, 682–692. [CrossRef] [PubMed]
57. Fleddermann, J.; Pichert, A.; Arnhold, J. Interaction of Serine Proteases from Polymorphonuclear Leucocytes with the Cell Surface and Heparin. *Inflammation* **2012**, *35*, 81–88. [CrossRef]
58. Belorgey, D.; Bieth, J.G. DNA Binds Neutrophil Elastase and Mucus Proteinase Inhibitor and Impairs Their Functional Activity. *FEBS Lett.* **1995**, *361*, 265–268. [CrossRef]
59. Lin, S.J.; Dong, K.C.; Eigenbrot, C.; Van Lookeren Campagne, M.; Kirchhofer, D. Structures of Neutrophil Serine Protease 4 Reveal an Unusual Mechanism of Substrate Recognition by a Trypsin-Fold Protease. *Structure* **2014**, *22*, 1333–1340. [CrossRef]
60. Morla, S.; Sankaranarayanan, N.V.; Afosah, D.K.; Kumar, M.; Kummarapurugu, A.B.; Voynow, J.A.; Desai, U.R. On the Process of Discovering Leads That Target the Heparin-Binding Site of Neutrophil Elastase in the Sputum of Cystic Fibrosis Patients. *J. Med. Chem.* **2019**, *62*, 5501–5511. [CrossRef]
61. Motta, J.P.; Rolland, C.; Edir, A.; Florence, A.C.; Sagnat, D.; Bonnart, C.; Rousset, P.; Guiraud, L.; Quaranta-Nicaise, M.; Mas, E.; et al. Epithelial Production of Elastase Is Increased in Inflammatory Bowel Disease and Causes Mucosal Inflammation. *Mucosal. Immunol.* **2021**, *14*, 667–678. [CrossRef]
62. Schuliga, M.; Westall, G.; Xia, Y.; Stewart, A.G. The Plasminogen Activation System: New Targets in Lung Inflammation and Remodeling. *Curr. Opin. Pharmacol.* **2013**, *13*, 386–393. [CrossRef] [PubMed]
63. Li, Q.; Ke, F.; Zhang, W.; Shen, X.; Xu, Q.; Wang, H.; Yu, X.Z.; Leng, Q.; Wang, H. Plasmin Plays an Essential Role in Amplification of Psoriasiform Skin Inflammation in Mice. *PLoS ONE* **2011**, *6*, e16483. [CrossRef] [PubMed]
64. Voynow, J.A.; Shinbashi, M. Neutrophil Elastase and Chronic Lung Disease. *Biomolecules* **2021**, *11*, 1065. [CrossRef] [PubMed]
65. Baker, S.K.; Strickland, S. A Critical Role for Plasminogen in Inflammation. *J. Exp. Med.* **2020**, *217*, e20191865. [CrossRef] [PubMed]
66. Al-Horani, R.A.; Abdelfadiel, E.I.; Afosah, D.K.; Morla, S.; Sistla, J.C.; Mohammed, B.; Martin, E.J.; Sakagami, M.; Brophy, D.F.; Desai, U.R. A Synthetic Heparin Mimetic That Allosterically Inhibits Factor XIa and Reduces Thrombosis in Vivo without Enhanced Risk of Bleeding. *J. Thromb. Haemost.* **2019**, *17*, 2110–2122. [CrossRef]

Disclaimer/Publisher's Note: The statements, opinions and data contained in all publications are solely those of the individual author(s) and contributor(s) and not of MDPI and/or the editor(s). MDPI and/or the editor(s) disclaim responsibility for any injury to people or property resulting from any ideas, methods, instructions or products referred to in the content.